RESEARCH MEMORANDUM

TRANSONIC WIND-TUNNEL INVESTIGATION OF AN UNSWEPT WING IN COMBINATION WITH A SYSTEMATIC SERIES OF FOUR BODIES

By Bruce B. Estabrooks

Langley Aeronautical Laboratory
Langley Field, Va.

NATIONAL ADVISORY COMMITTEE
FOR AERONAUTICS

WASHINGTON

January 6, 1953
Declassified November 14, 1956

NATIONAL ADVISORY COMMITTEE FOR AERONAUTICS

RESEARCH MEMORANDUM

TRANSONIC WIND-TUNNEL INVESTIGATION OF AN UNSWEPT WING IN COMBINATION WITH A SYSTEMATIC SERIES OF FOUR BODIES

By Bruce B. Estabrooks

SUMMARY

A wing having 0° sweepback of the 0.25-chord line has been investigated in conjunction with a systematic series of bodies at Mach numbers from 0.60 to 1.13 in the Langley 8-foot transonic tunnel. The wing had an aspect ratio of 4, taper ratio of 0, and 4-percent-thick, symmetrical airfoil sections parallel to the model plane of symmetry. The airfoil sections consist of circular arcs with the maximum thickness at the 0.40-chord stations. The series of bodies consisted of a body of revolution having a curved profile from the nose to the base, and various modifications of this basic body. The first modification had the forebody extended forward 2 diameters, the second had a cylindrical afterbody in place of the original afterbody, and the third modification was a combination of the first and second modifications resulting in a cylindrical section extending from the vicinity of the wing leading edge to the base of the model.

The wing-body interference effects on the aerodynamic characteristics of the unswept wing were most pronounced in the transonic speed range, and the drag was most significantly affected. At low lift coefficients, the drag rise of the wing with interference was reduced approximately 20 to 30 percent by the addition of the cylindrical afterbody to the basic model at a Mach number of 1.00. The maximum lift-drag ratio for the wing when in combination with the curved afterbody was increased approximately 20 percent by the substitution of the cylindrical afterbody at a Mach number of 1.00.

INTRODUCTION

Among the factors governing the aerodynamic characteristics of airplanes, especially in the transonic speed range, is the effect of wing-fuselage interference. As part of a program studying the wing-fuselage

interference effects on the aerodynamic characteristics of wing-fuselage combinations at transonic speeds, a series of representative wings has been investigated in combination with a systematic series of four bodies. Various modifications to the basic body were made in an effort to reduce the effects of interference between the wing and the body. The forebody was extended forward in an attempt to reduce the induced velocities produced by the body in the region of the forward portion of the wing. A cylindrical afterbody was added in an attempt to reduce the induced velocities and adverse gradients produced by the original afterbody in the region of the rear part of the wing. A sweptback wing tested in conjunction with the series of bodies has been reported in reference 1. In the present investigation, an unswept wing has been tested in conjunction with the same series of bodies. The unswept wing was designed on the basis of structural as well as aerodynamic considerations to be optimum for utilization at supersonic speeds as well as transonic speeds. The results provide an indication of the aerodynamic characteristics of such an unswept wing in the transonic speed range as well as the effects of several basic changes in body shape on wing-fuselage interference.

The results have been obtained at Mach numbers from 0.60 to 1.13 for the angle-of-attack range from 0° to 7°.

SYMBOLS

c	wing local chord
$\bar{c}$	wing mean aerodynamic chord, in.
C_D	drag coefficient, D/qS
C_{D_o}	drag coefficient at zero lift
C_L	lift coefficient, L/qS
C_m	pitching-moment coefficient, $M_{\bar{c}/4}/qS\bar{c}$
$dC_L/d\alpha$	lift-curve slope per degree
D	drag, lb
L	lift, lb
$(L/D)_{max}$	maximum lift-drag ratio

M	free-stream Mach number
$M_{\bar{c}/4}$	pitching moment about 0.25$\bar{c}$ station, in-lb
P_b	base pressure coefficient, $\frac{P_b - P_o}{q}$
ΔP_b	incremental base pressure coefficient due to addition of wing to fuselage
p_b	static pressure at model base, lb/sq ft
p_o	free-stream static pressure, lb/sq ft
q	free-stream dynamic pressure, $\rho V^2/2$, lb/sq ft
S	wing plan-form area to center line of model, sq ft
t	wing local thickness
V	free-stream velocity
α	angle of attack of fuselage center line, deg
ρ	free-stream density
$\partial C_m/\partial C_L$	static-longitudinal-stability parameter

APPARATUS AND METHODS

Tunnel

The transonic data were obtained in the Langley 8-foot transonic tunnel which is a dodecagonal, slotted-throat, single-return wind tunnel designed to obtain aerodynamic data through the speed of sound without the usual effects of choking and blockage. A complete description of the Langley 8-foot transonic tunnel may be found in reference 2 and complete calibrations of the tunnel are presented in reference 3.

Models

Wing.- The wing used in this investigation had 0° sweepback of the 0.25-chord line, an aspect ratio of 4, a taper ratio of 0, and 4-percent-thick, symmetrical airfoil sections parallel to the model plane of symmetry. The airfoil sections consisted of circular arcs with the maximum

thickness of the sections at the 0.40-chord stations. The wing was tested at a midwing position on the fuselage at 0° incidence. Dimensional details of the model are presented in figure 1 and photographs of typical wing-fuselage configurations are shown in figure 2. The wing was constructed of 14S-T aluminum alloy.

Bodies.- The body of the basic wing-fuselage configuration was a body of revolution, shown as solid lines in figure 1, with a basic fineness ratio of 12, although an actual fineness ratio of 9.8 was obtained after cutting off approximately one-sixth of the body to attach the tapered sting of the internal strain-gage balance. The basic fuselage was designed to produce relatively low induced velocities and the body ordinates are presented in reference 1. The basic wing-fuselage combination is referred to as configuration A.

The three additional bodies used in the investigations were systematic modifications of the fuselage of configuration A. The first modification (configuration B) had the original forebody of the basic model extended forward a distance of 2 diameters and a cylindrical midsection placed between the extended forebody and the original afterbody (fig. 1). The second modification (configuration C) was obtained by substituting a cylindrical afterbody for the afterbody of configuration A from the maximum diameter rearward to the end of the fuselage. The third modification to the basic model (configuration D) was obtained by combining the extended forebody of configuration B and the cylindrical afterbody of configuration C. The fineness ratio of the bodies of configurations B and D was 11.8. The ordinates of the bodies of the four wing-fuselage combinations are presented in reference 1.

The fuselage of the basic model was of hollow steel construction. The modifications to the model were constructed of a plastic material.

Model Support System

An internal, electrical strain-gage balance was secured to the body of each configuration at its forward end. The rear portion of the balance consisted of a sting that supported the model near the center of the tunnel. For the models with the original afterbody, the sting was tapered from the model base rearward. The sting rearward of the base of the cylindrical afterbody was cylindrical with a diameter slightly less than that of the body (note fig. 1).

The support system and the angle-of-attack mechanism are described in reference 4. In order to keep the model reasonably close to the tunnel axis when the angle of attack was varied from 0° to 7°, a 5° coupling was installed ahead of the pivot point of the sting. Consequently, at 0° angle of attack, the model was offset from the tunnel axis slightly.

Test Conditions and Accuracy

The flow in the region of the test section occupied by the model was satisfactorily uniform at all test Mach numbers. Deviations from the average free-stream Mach number did not exceed 0.003 at subsonic speeds, and were not more than 0.010 with further increase in Mach number to 1.13 (ref. 3).

Lift, drag, and pitching moment were determined by means of an internal strain-gage balance. From the static calibrations and reproducibility of the data, the measured coefficients were estimated to be accurate within the following limits:

	Subsonic speeds	Transonic speeds
C_L	±0.008	±0.004
C_D	±0.001	±0.0005
C_m	±0.004	±0.002

The inaccuracies presented are judged to be the maximum deviations and, in general, the accuracy of the measured coefficients may be expected to be much better. Base pressures were determined as the average of readings from static-pressure orifices located on the top and the bottom of the sting in the plane of the model base. The base pressure coefficient was estimated to be accurate within ±0.003.

The angle of attack of the model was measured by a cathetometer sighted on a reference line on the side of the fuselage and was judged to be accurate to within $\pm 0.10^{\circ}$.

The axially slotted test section minimizes boundary interference due to solid blockage (ref. 5), and the effects of wake blockage are similarly reduced. Therefore, the usual corrections to the Mach number and dynamic pressure for the effects of model and wake blockage and to the drag coefficients for the effect of the pressure gradient caused by the wake are no longer applied. However, there was a range of Mach numbers above 1.0 where shocks and expansions from the model nose were reflected back to the surface of the model by the test-section boundary. On the basis of the results of reference 4, the boundary-reflected disturbances had negligible effects on the lift and pitching-moment coefficients, increased the drag coefficient as much as 0.002 at a Mach number of approximately 1.04, and decreased it as much as 0.002 at a Mach number of approximately 1.09. However, since the data presented herein are for a wing with interference, any noticeable effects of reflections onto the body should be largely eliminated when the body data are subtracted from the data for the wing-body combination. The configurations employing the 9.8-fineness-ratio body were free of wall interference effects at Mach

numbers of 1.09 and above. The boundary-reflected disturbances did not clear the configuration employing the 11.8-fineness-ratio body up to the highest Mach number investigated.

The variation of Reynolds number with Mach number, based on the wing mean aerodynamic chord of 8.0 inches, varied from 2.3×10^6 to 2.7×10^6 with increases in Mach number from 0.60 to 1.13.

RESULTS

The data presented herein are for the wing with wing-fuselage interference. The wing-with-interference results were obtained by subtracting algebraically the fuselage-alone data from the wing-fuselage data. The fuselage-alone data have been presented in reference 1. The wing-fuselage interference includes the effect of the wing on the body as well as the effect of the body on the wing.

The drag coefficients presented herein have been adjusted to the condition of free-stream static pressure at the model base. The base pressure coefficients for the fuselage alone (ref. 1) were subtracted algebraically from those for the wing-body combination (fig. 3(a)) to obtain the incremental pressure-coefficient values due to the addition of the wing to the fuselage (fig. 3(b)).

Angles of attack, drag coefficients, and pitching-moment coefficients for the wing with interference for the four configurations (A, B, C, and D) are presented in figure 4 as functions of lift coefficient. In order to facilitate presentation of the data, staggered scales have been used in figure 4 and care should be taken in selecting the zero axis for each curve.

From the basic data (figs. 4(a), 4(b), and 4(c)) all of the analyses (figs. 5 to 10) have been prepared. In several figures, symbols are used for clarity to identify the curves of the several configurations tested and do not necessarily indicate actual test points. The adjusted $(L/D)_{max}$ values (presented in fig. 8) were obtained by adding a uniform drag coefficient of 0.01 to all of the drag-coefficient data for the wing with interference.

DISCUSSION

The various modifications to the basic model were made in an effort to reduce the effects of interference between the wing and the body. The forebody was extended forward in an attempt to reduce the induced velocities produced by the body in the region of the forward portion of the

wing. The cylindrical afterbody was added in an attempt to reduce the induced velocities and adverse gradients produced by the original afterbody in the region of the rear part of the wing.

Lift Characteristics

The effects of interference on the lift-curve slopes of the wing averaged over the lift-coefficient range from 0 to 0.4 are presented in figure 5. The basic model (configuration A) experienced an increase in lift-curve slope of the order of 40 percent with increase in Mach number from 0.60 to approximately 1.0, followed by a reduction in lift-curve slope of about 7 percent with increase in Mach number to 1.13. The addition of the extended forebody and cylindrical midsection to the basic model to form configuration B decreased the lift-curve slopes throughout the Mach number range investigated, the reduction being as much as 6 percent in the transonic speed range. No satisfactory explanation has been found for this reduction of lift-curve slope. The addition of the cylindrical afterbody to configurations A and B to form configurations C and D improved the lift-curve slopes by about 7 percent in the transonic Mach number range. This is probably due to the favorable influence of the cylindrical afterbody on the flow over the rear portion of the wing. The cylindrical afterbody tended to reduce the adverse pressure gradients over the rear portions of the wing, and thereby reduce the extent of separated flow over these sections. (See ref. 6.)

Drag Characteristics

The effects of wing-body interference on the drag characteristics of the wing are presented in figure 6 for lift coefficients of 0, 0.2, and 0.4. At a lift coefficient of 0, the basic model (configuration A) experienced a drag-coefficient rise of approximately 0.014 with increase in Mach number from 0.90 to 1.00, due primarily to shock losses rather than to separation losses over this thin unswept wing. (See ref. 7.) With further increase in Mach number to 1.13, the basic model experienced some reductions in drag coefficient to a value of 0.0155. At a lift coefficient of 0, the addition of the extended forebody (configuration B) caused a slight increase in the interference drag in the subsonic speed range and reduced the maximum drag rise. The addition of the cylindrical afterbody to the basic model (configuration C) caused a slight increase in drag in the subsonic Mach number range, but reduced the maximum drag rise appreciably. The configuration employing both the extended forebody and the cylindrical afterbody (configuration D) had nearly the same variations with Mach number as noted for the zero-lift drag of configuration B up to a Mach number of 1.025. With further increase in Mach number to 1.13, configuration D experienced erratic variations of zero-lift drag. It had been expected that configuration D would experience reductions in drag in the transonic speed range roughly equal to the summation

of the drag reductions associated with configurations B and C. No explanation can be made as to why this was not realized above a Mach number of 1.025.

At a lift coefficient of 0.2, the drag-coefficient rise associated with an increase in Mach number to 1.00 for the basic model (configuration A) was approximately the same as at a lift coefficient of 0. The addition of the extended forebody to the basic model (configuration B) caused a slight decrease in the drag in the transonic speed range. The interference-drag losses associated with the curved afterbody of the basic model were reduced approximately 30 percent by the addition of the cylindrical afterbody at a Mach number of 1.00. The drag characteristics of the configuration employing both the extended forebody and cylindrical afterbody (configuration D) were more consistent at a lift coefficient of 0.2 than at a lift coefficient of 0 in that for the transonic speed range this configuration experienced drag reductions that were equal to the sum of the drag reductions experienced by the separate modifications.

The favorable interference effect of the cylindrical afterbody may be attributed to the less rapid variation of the cross-sectional area of the bodies employing the cylindrical afterbody as compared with those with the original afterbody (fig. 11). This less rapid variation results in a reduction in the induced velocities over the afterbody and reduction of the shock losses for the combination. It has been concluded in reference 6 that the zero-lift drag rise near the speed of sound of wing-fuselage combinations with thin, low-aspect-ratio wings is dependent upon the axial distribution of the cross-sectional areas.

At a lift coefficient of 0.4, the four configurations experienced reductions in the drag of the order of 25 percent with increase in Mach number from 0.60 to 0.85. This reduction of drag was associated with the increase in lift-curve slope noted in the discussion of figure 5. The basic model (configuration A) experienced a drag increase of approximately 50 percent with increase in Mach number from 0.85 to 1.0 due to shock and separation losses over the wing.

Although the addition of the extended forebody to the sweptback-wing—fuselage combination of reference 1 improved the interference drag characteristics at a lift coefficient of 0.4 throughout the speed range investigated, this favorable effect was not realized for the unswept-wing—fuselage combination. Instead, the addition of the extended forebody to the unswept-wing—fuselage combination (configuration B) increased the drag by about 10 percent in the transonic speed range. The higher drag values are probably associated with the lower lift-curve slopes that are indicated for this configuration in figure 5. The addition of the cylindrical afterbody to the basic model (configuration C) caused reductions in the drag rise of the order of 20 percent throughout the transonic speed range. This reduction of drag was probably contributed to by the

reduction of separation over the rear portion of the wing associated with the less adverse pressure gradients in the flow about the cylindrical afterbody.

Lift-Drag Ratio

The maximum lift-drag ratio (fig. 7) of the basic model (configuration A) decreased from 20.2 to 8.6 with increase in Mach number from 0.85 to 1.00, and then increased slightly with further increase in Mach number to 1.13. The extended forebody had little effect on the lift-drag ratios of the wing with interference throughout the speed range. The favorable influence of the cylindrical afterbody on the drag for lifting conditions in the transonic speed range leads to higher maximum lift-drag ratios as shown in figure 7. At a Mach number of 1.00, the use of this cylindrical afterbody increased the $(L/D)_{max}$ values from 8.6 for configuration A to approximately 11.0 for configurations C and D.

The variations with Mach number of an adjusted maximum lift-drag ratio are presented in figure 8 for the four configurations. The adjusted $(L/D)_{max}$ values were obtained by the addition of 0.01 to the drag coefficients of the experimental data. This value approximates the additional drag that might occur if a fuselage, canopy, empennage, and other protuberances were added to the wing to form a real configuration. Therefore, the adjusted $(L/D)_{max}$ values were obtained at more realistic values of lift coefficient. The extended forebody did not improve the adjusted $(L/D)_{max}$ values through the transonic speed range, whereas the cylindrical afterbody caused an increase in adjusted $(L/D)_{max}$ of the order of 14 percent in the transonic speed range.

Pitching Moment

The variation with Mach number of the pitching-moment coefficients (fig. 9) for lifting conditions indicates that the four configurations experienced a similar rearward movement of the center of pressure with increase in Mach number to unity. Generally, the extended forebody had little effect on the pitching-moment characteristics throughout the speed range investigated. The cylindrical afterbody caused interference effects that resulted in a more forward position of the center of pressure throughout the Mach number range at lift coefficients of 0.2 and 0.4. This result may be attributed primarily to the interference effects of the wing on the body; that is, the downwash behind the wing reduced the positive load on the cylindrical afterbody, thereby contributing to more positive values of pitching moment.

The effects of Mach number variation on the static-longitudinal-stability parameter $\partial C_m/\partial C_L$ for the wing with interference are shown

in figure 10. In general, at lift coefficients of 0, 0.2, and 0.4 the four configurations experienced negative trends of $\partial C_m/\partial C_L$ for the wing with interference as the Mach number approached 1.00. The addition of the extended forebody (configuration B) had little influence on $\partial C_m/\partial C_L$ through the transonic speed range at all lift coefficients. The utilization of the cylindrical afterbody (configurations C and D) changed the value of $\partial C_m/\partial C_L$ by 0.05 in the positive direction in the transonic speed range at lift coefficients of 0 and 0.2, and caused little or no change at a lift coefficient of 0.4.

CONCLUSIONS

The investigation of an unswept wing in combination with a systematic series of bodies has led to the following conclusions relative to wing-body interference:

1. The wing-body interference effects on the aerodynamic characteristics of the unswept wing were most pronounced in the transonic speed range, and the drag was most significantly affected.

2. The drag rise of the wing with interference at lift coefficients of 0 to 0.4 was reduced approximately 20 to 30 percent by the substitution of the cylindrical afterbody for the curved original afterbody at a Mach number of 1.00. This reduction may be attributed to a decrease in shock losses for the combination.

3. The maximum lift-drag ratio for the wing when in combination with the curved original afterbody was increased approximately 20 percent by the substitution of a cylindrical afterbody at a Mach number of 1.00.

4. The addition of a cylindrical afterbody to the body of the original wing-fuselage combination caused a small increase in lift-curve slope in the transonic speed range and shifted the center of pressure forward throughout the Mach number range.

Langley Aeronautical Laboratory,
National Advisory Committee for Aeronautics,
Langley Field, Va.

REFERENCES

1. Loving, Donald L., and Wornom, Dewey E.: Transonic Wind-Tunnel Investigation of the Interference Between a 45° Sweptback Wing and a Systematic Series of Four Bodies. NACA RM L52J01, 1952.

2. Wright, Ray H., and Ritchie, Virgil S.: Characteristics of a Transonic Test Section With Various Slot Shapes in the Langley 8-Foot High-Speed Tunnel. NACA RM L51H10, 1951.

3. Ritchie, Virgil S., and Pearson, Albin O.: Calibration of the Slotted Test Section of the Langley 8-Foot Transonic Tunnel and Preliminary Experimental Investigation of Boundary-Reflected Disturbances. NACA RM L51K14, 1952.

4. Osborne, Robert S., and Mugler, John P., Jr.: Aerodynamic Characteristics of a 45° Sweptback Wing-Fuselage Combination and the Fuselage Alone Obtained in the Langley 8-Foot Transonic Tunnel. NACA RM L52E14, 1952.

5. Wright, Ray H., and Ward, Vernon G.: NACA Transonic Wind-Tunnel Test Sections. NACA RM L8J06, 1948.

6. Whitcomb, Richard T.: A Study of the Zero-Lift Drag-Rise Characteristics of Wing-Body Combinations Near the Speed of Sound. NACA RM L52H08, 1952.

7. Whitcomb, Richard T., and Kelly, Thomas C.: A Study of the Flow Over a 45° Sweptback Wing-Fuselage Combination at Transonic Mach Numbers. NACA RM L52D01, 1952.

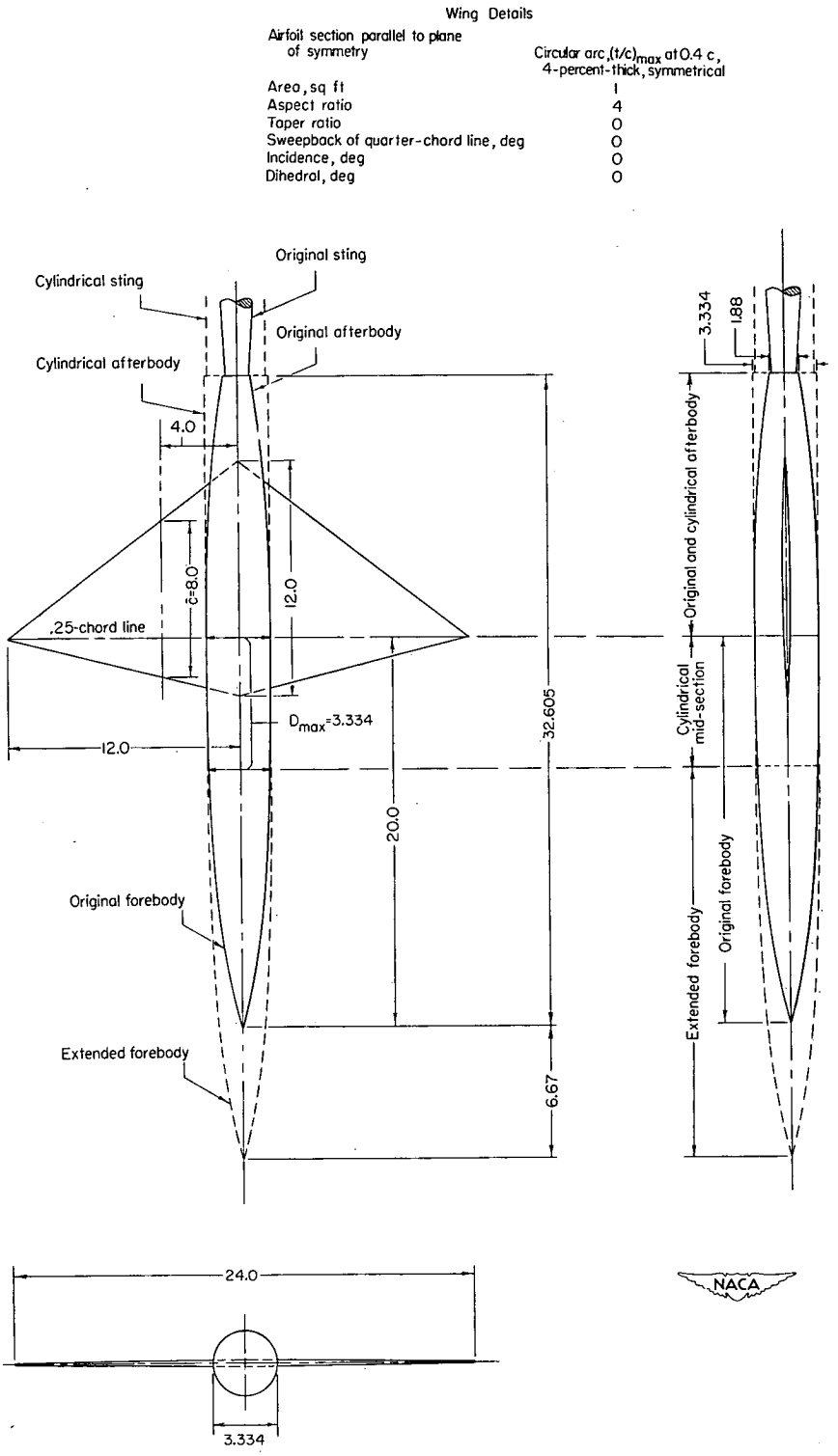

Figure 1.- Details of the wing-fuselage combination investigated in the slotted test section of the Langley 8-foot transonic tunnel. All dimensions are in inches.

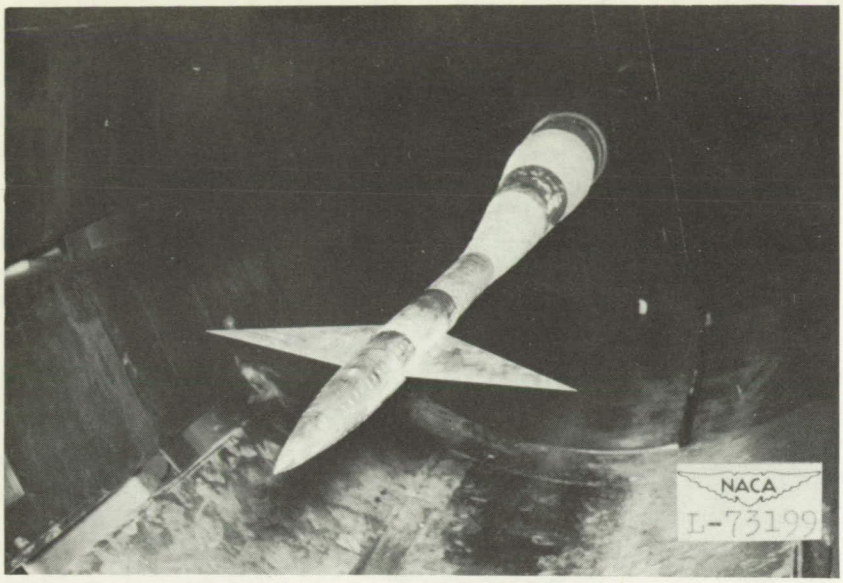

(a) Wing-body combination with original forebody and cylindrical afterbody (configuration C).

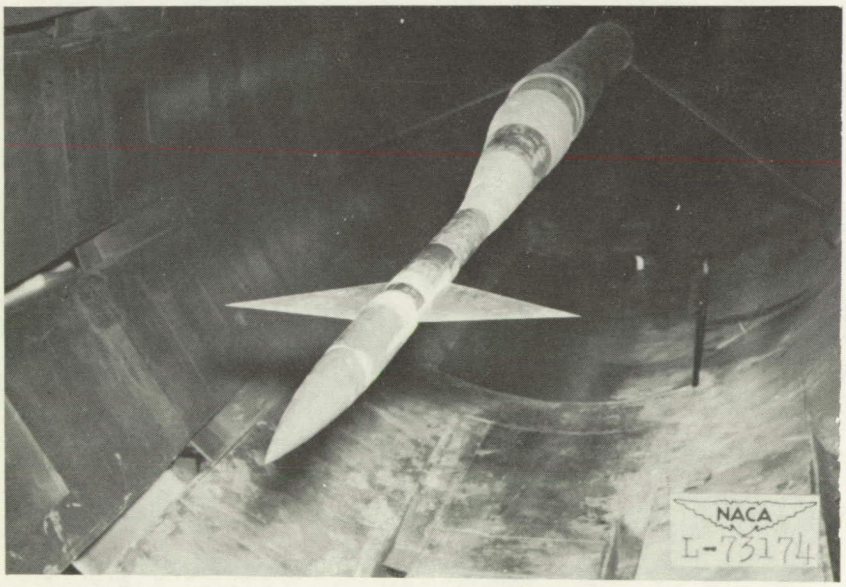

(b) Wing-body combination with extended forebody and cylindrical afterbody (configuration D).

Figure 2.- Typical wing-body combinations as tested in the Langley 8-foot transonic tunnel.

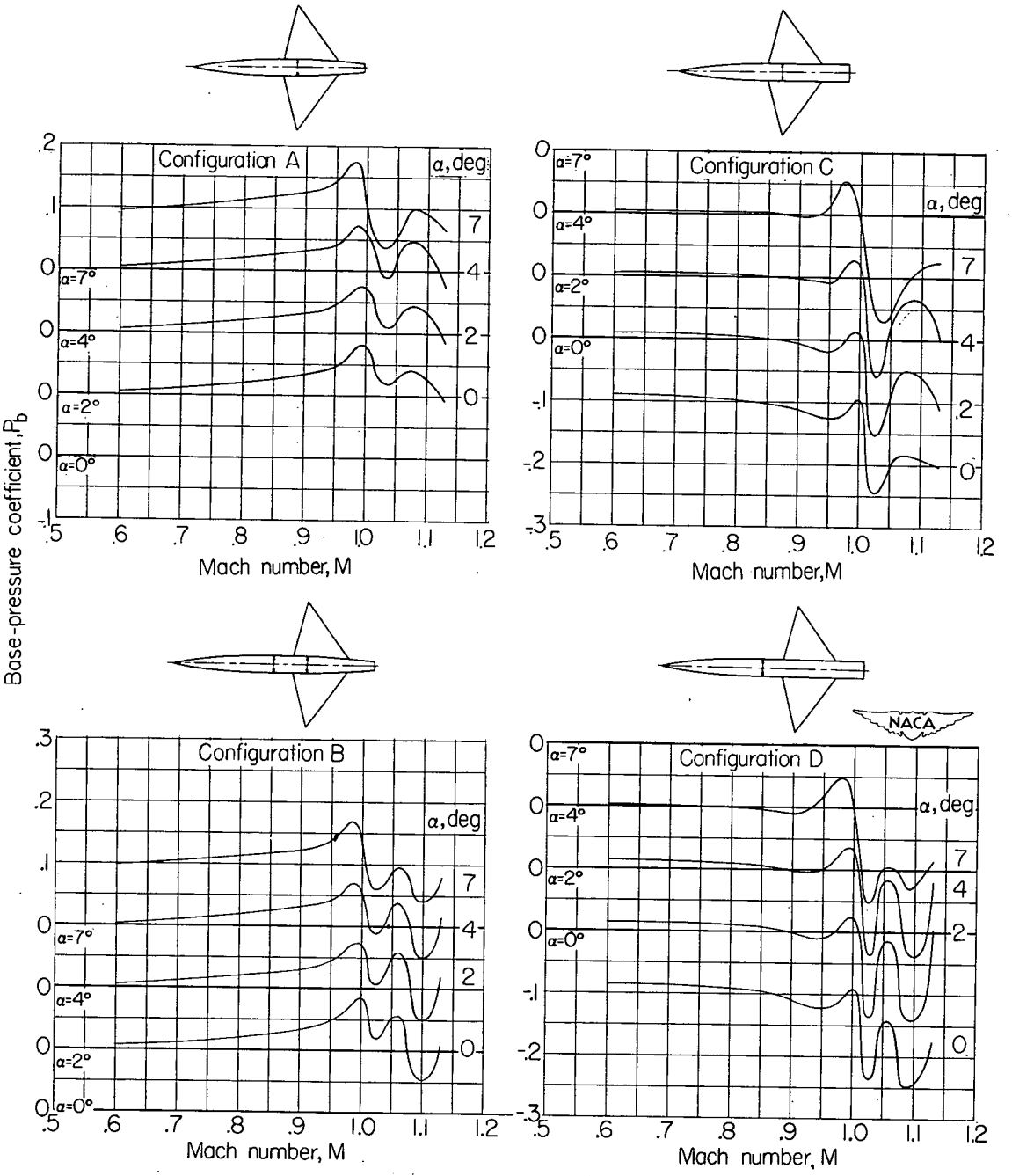

(a) Wing-body combinations.

Figure 3.- Variation with Mach number of the base pressure coefficient for the various configurations.

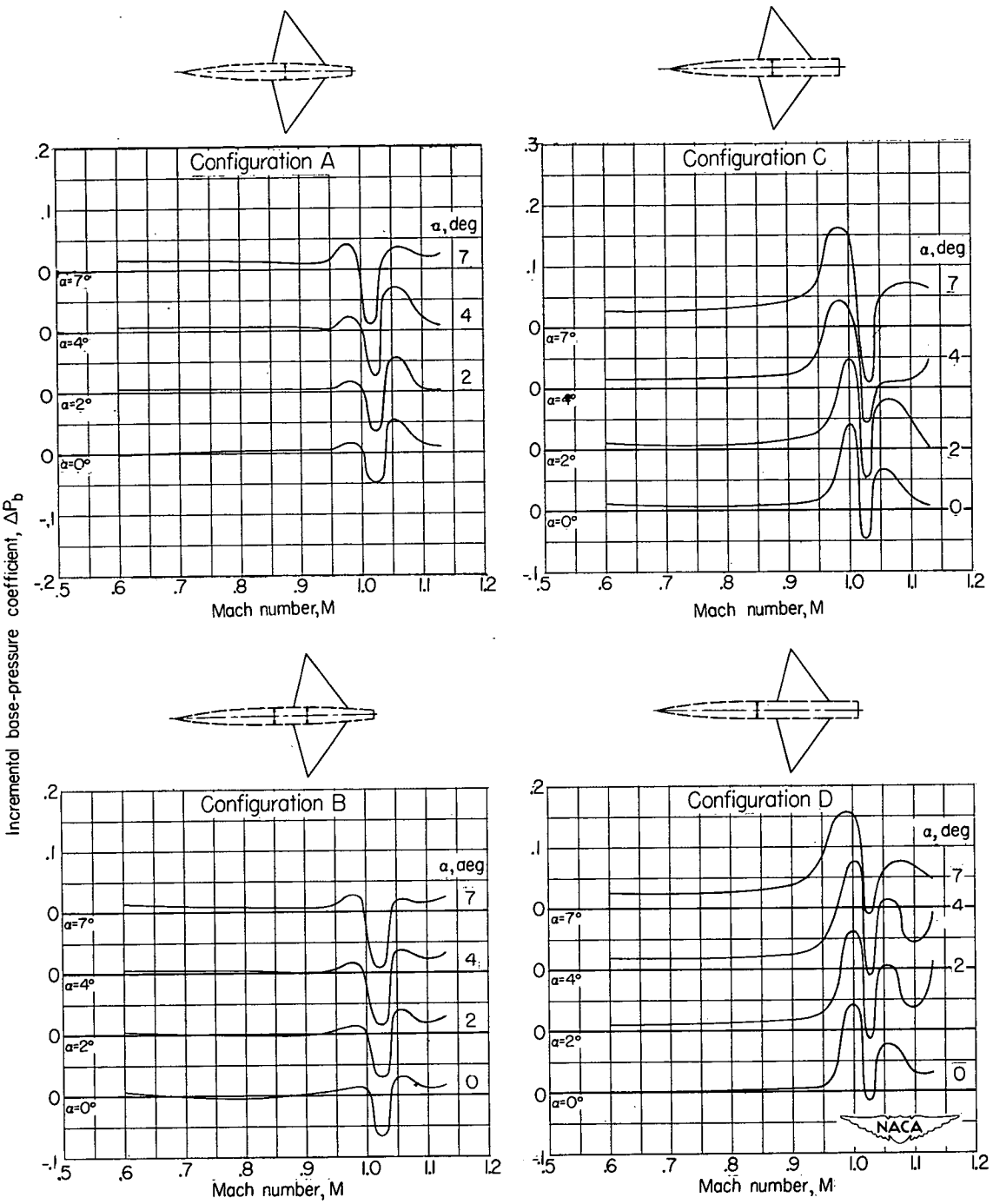

(b) Wing with wing-fuselage interference.

Figure 3.- Concluded.

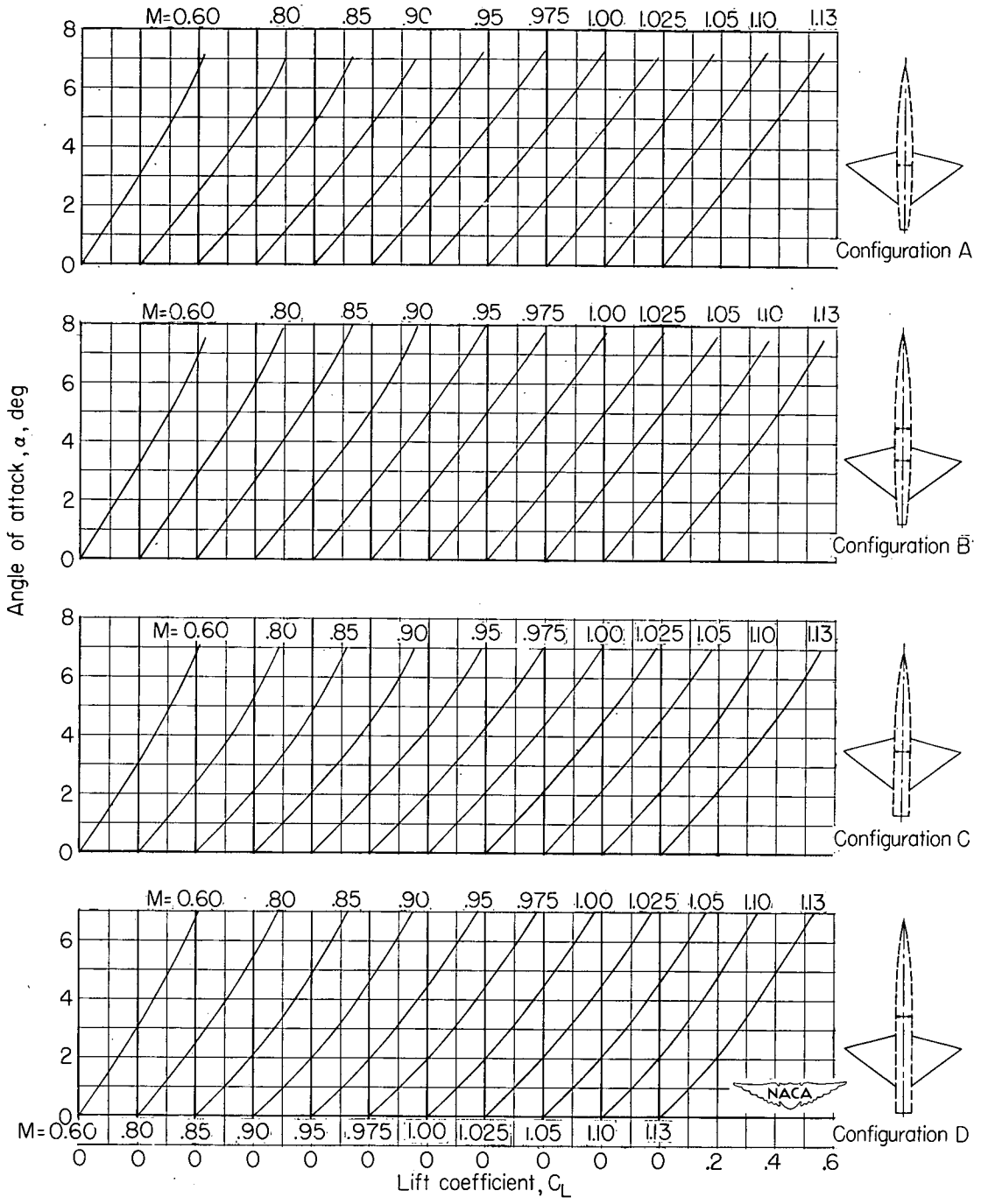

(a) Angle of attack.

Figure 4.- Variation with lift coefficient of the force and moment characteristics of the wing with wing-fuselage interference for the various configurations.

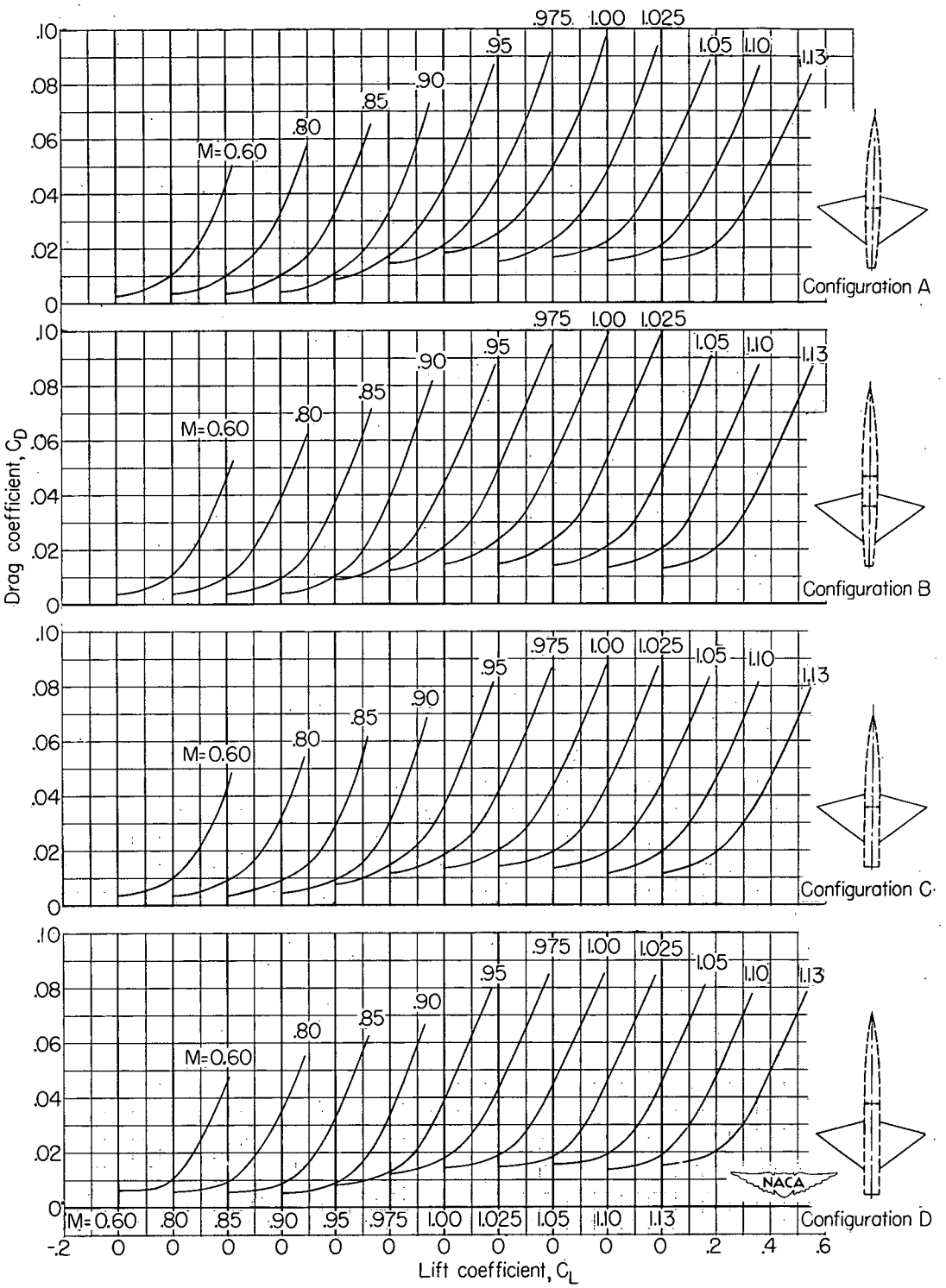

(b) Drag coefficient.

Figure 4.- Continued.

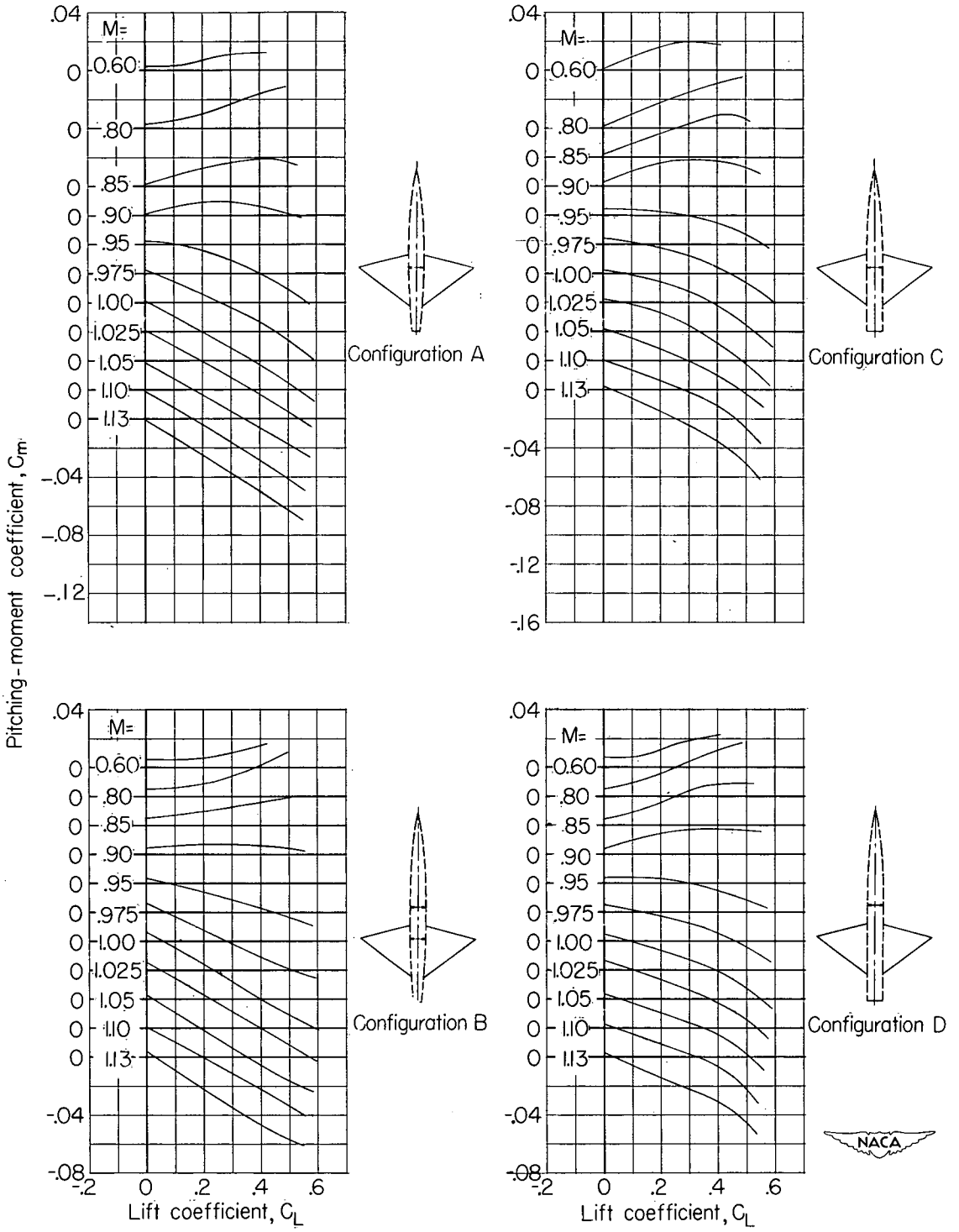

(c) Pitching-moment coefficient.

Figure 4.- Concluded.

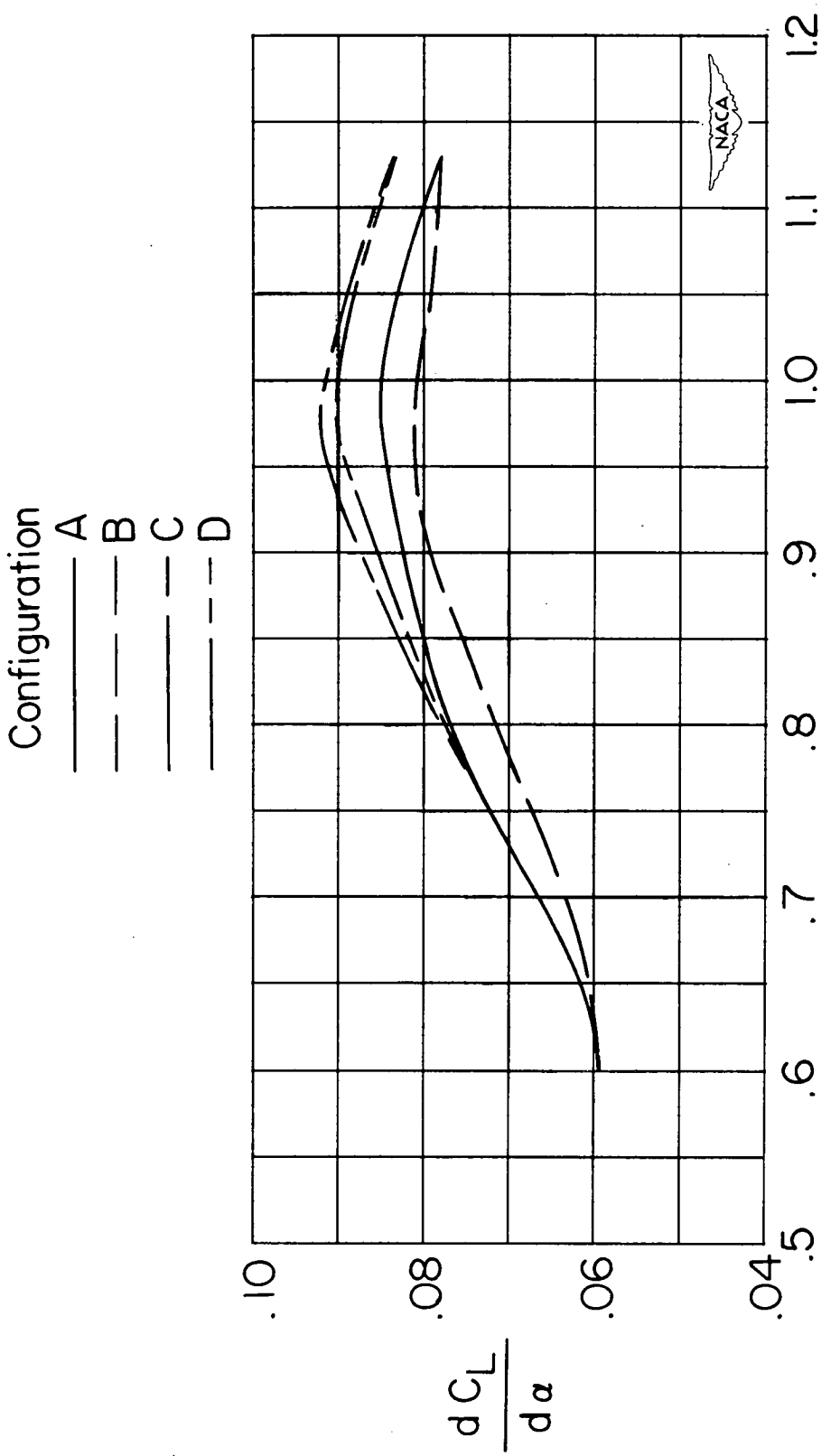

Figure 5.- Variation with Mach number of the mean lift-curve slopes for the wing with wing-fuselage interference for the various configurations.

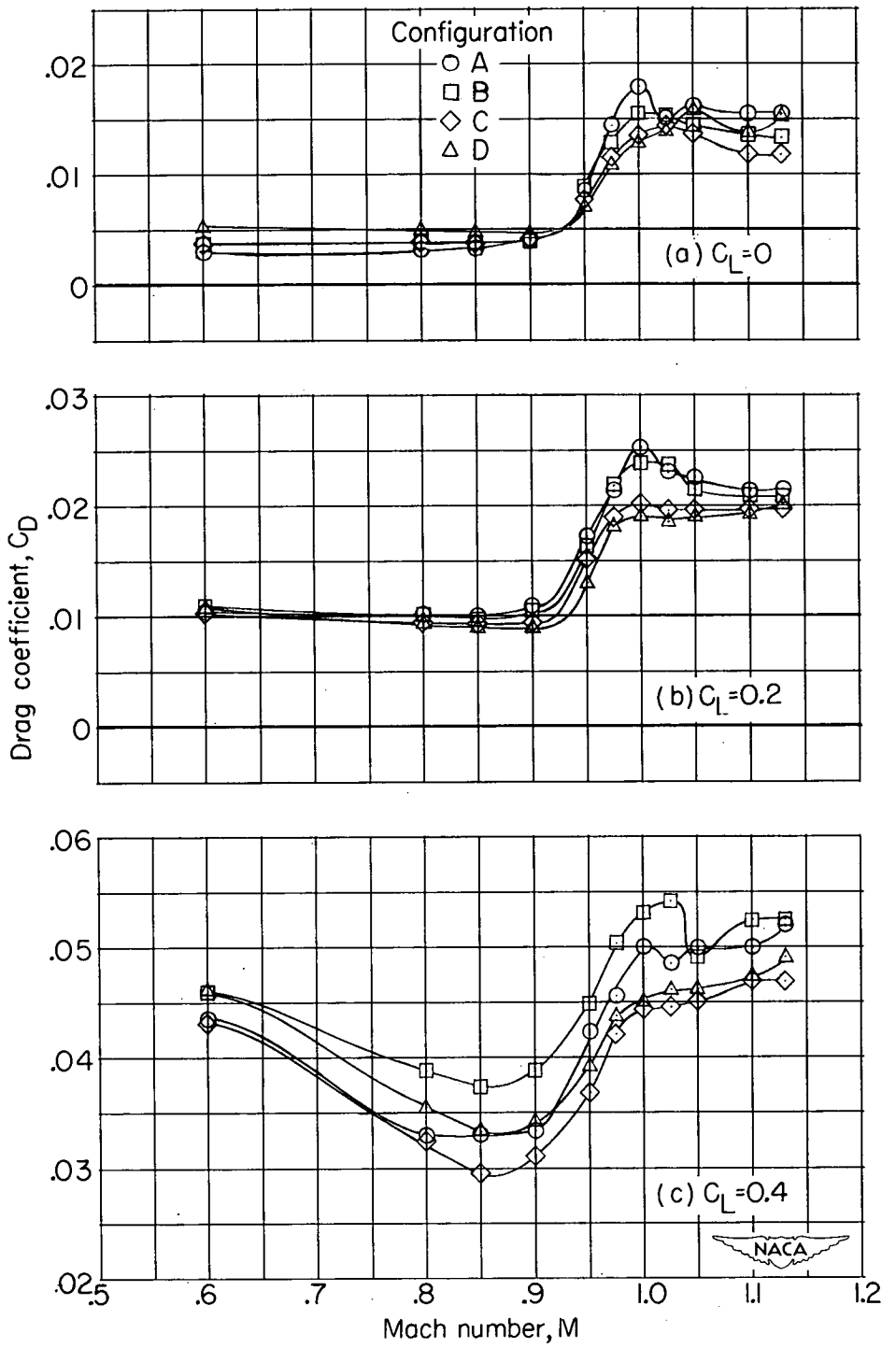

Figure 6.- Variation with Mach number of the drag coefficients of the wing with wing-fuselage interference for the various configurations at several lift coefficients. (Symbols are included for clarity rather than to indicate test points.)

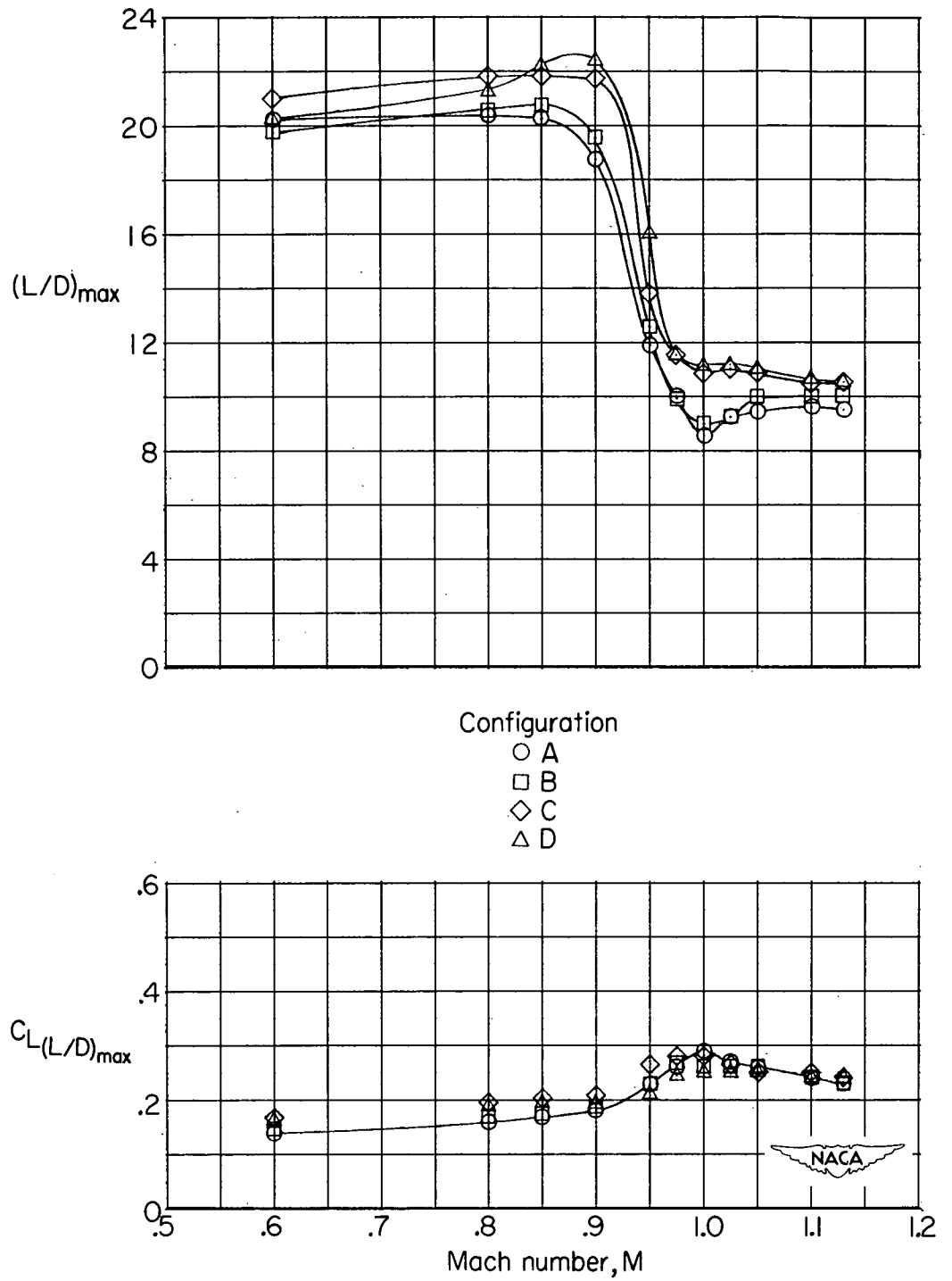

Figure 7.- Variation with Mach number of maximum lift-drag ratio and lift coefficient for maximum lift-drag ratio for the wing with wing-fuselage interference for the various configurations. (Symbols are included for clarity rather than to indicate test points.)

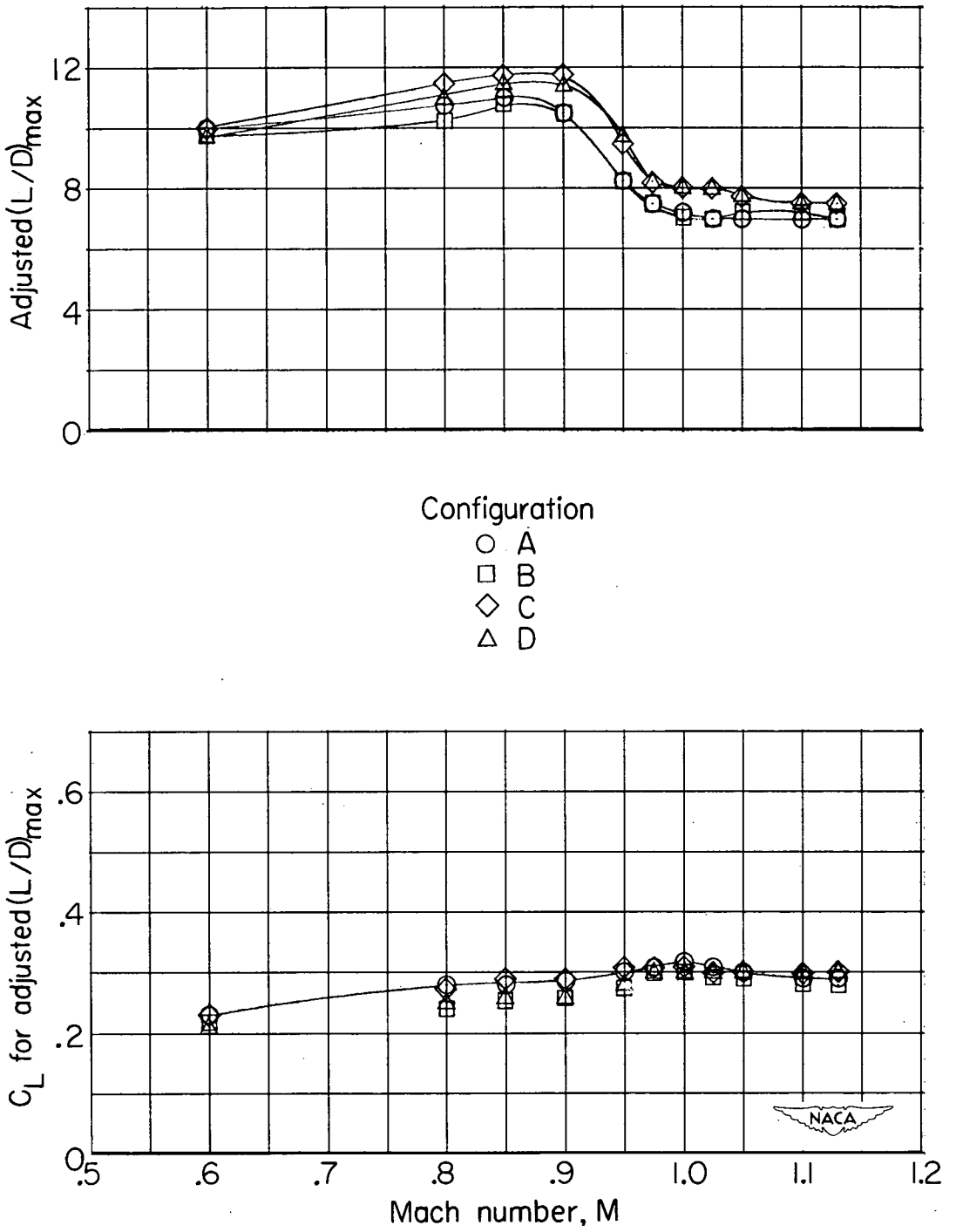

Figure 8.- Variation with Mach number of adjusted maximum lift-drag ratio and lift coefficient for adjusted maximum lift-drag ratio for the wing with wing-fuselage interference for the various configurations. (Symbols are included for clarity rather than to indicate test points.)

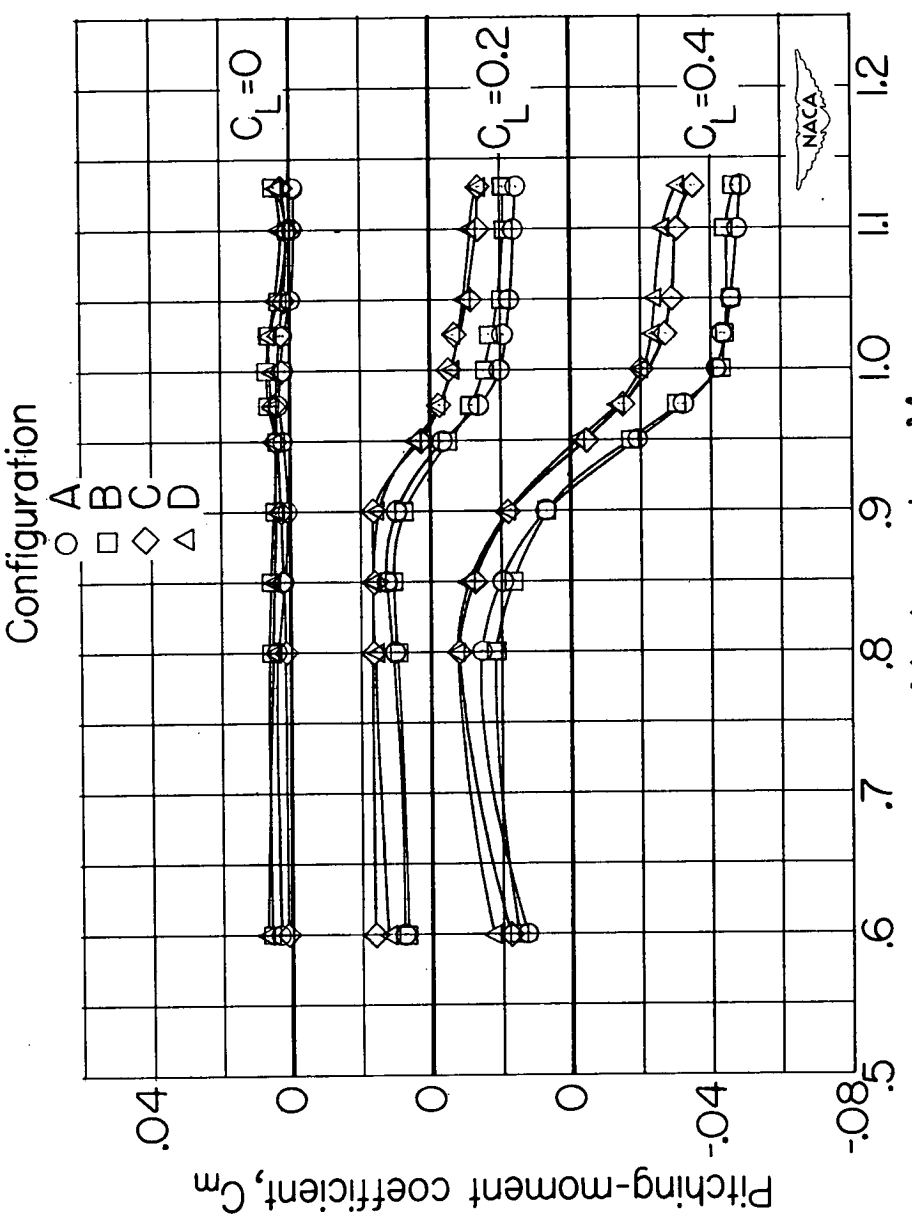

Figure 9.- Variation with Mach number of the pitching-moment coefficients of the wing with wing-fuselage interference for the various configurations at several lift coefficients. (Symbols are included for clarity rather than to indicate test points.)

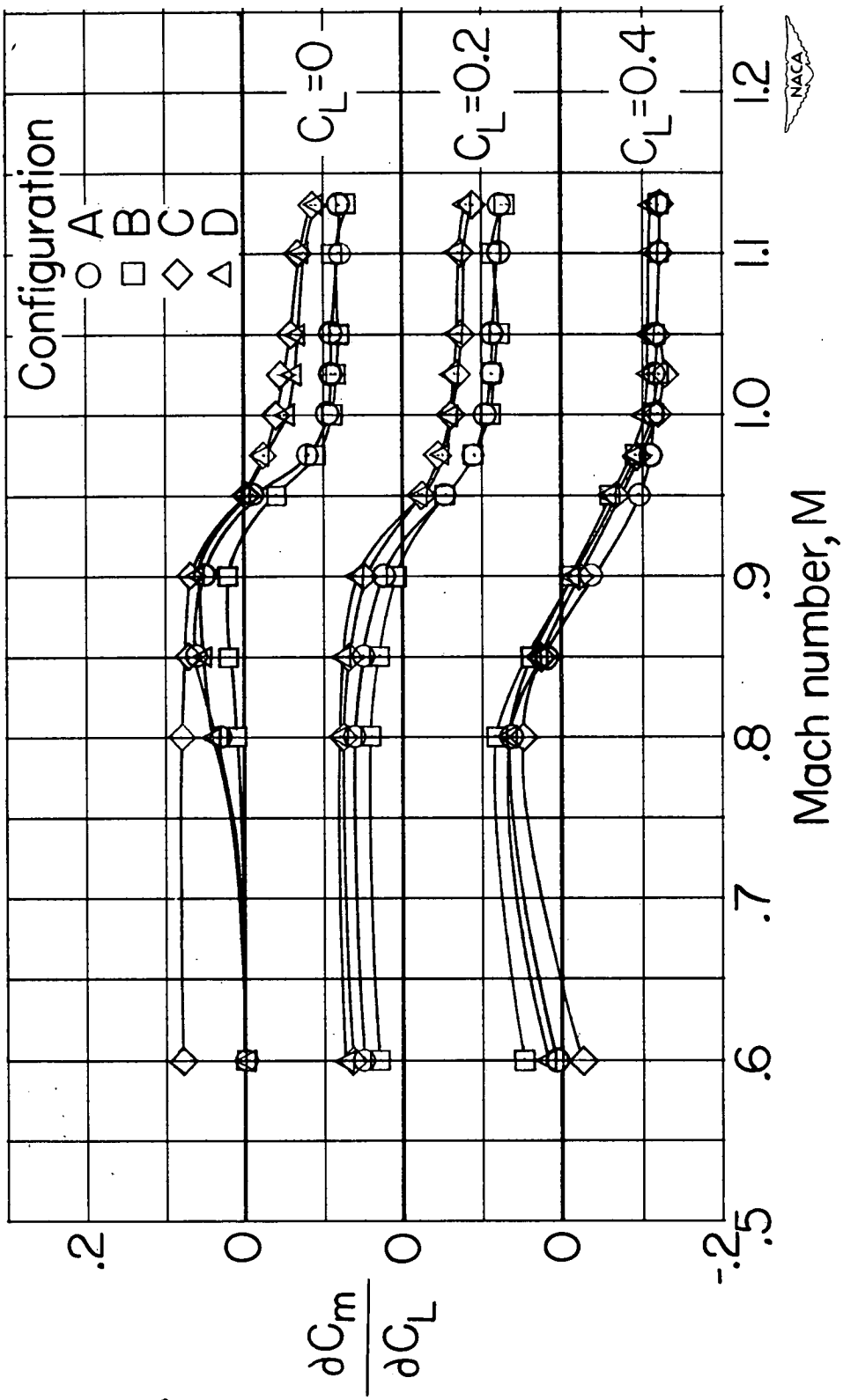

Figure 10.- Variation with Mach number of the static-longitudinal-stability parameter $\partial C_m/\partial C_L$ for the wing with wing-fuselage interference for the various configurations. (Symbols are included for clarity rather than to indicate test points.)

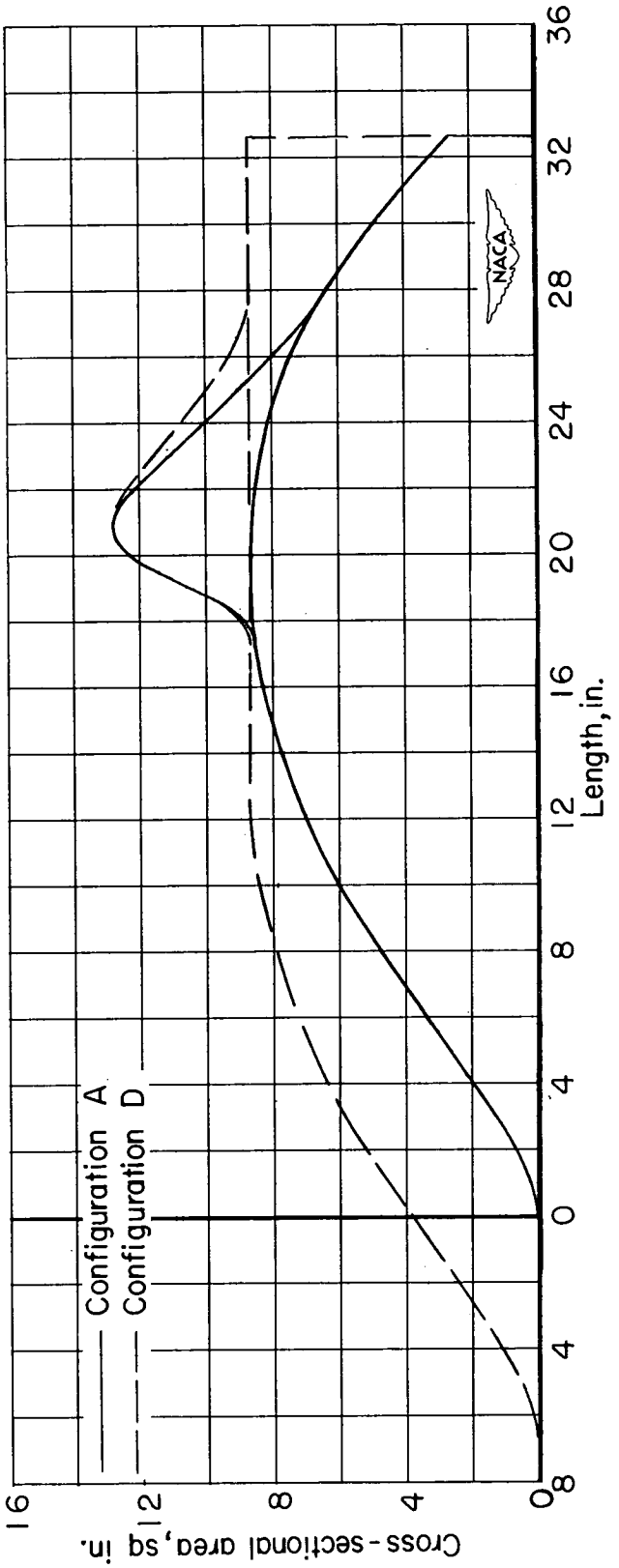

Figure 11.- Axial variations of the cross-sectional area normal to the model axis for two of the wing-body combinations tested. The zero point on the abscissa is the nose of the original body.